

Electron Polaron at Neutral 180° Domain Wall in PbTiO_3 : Stability, Trapping Energies, and Transverse Polarization

Mohammad Amirabbasi,^{1,*} Jochen Rohrer,¹ and Karsten Albe^{1,†}

¹*Technical University of Darmstadt, Materials Modelling Division,
Otto-Berndt-Straße 3, Darmstadt D-64287, Germany*

We use density-functional theory with a Hubbard correction to investigate Ti-centered electron polarons at neutral PbO-centered 180° domain walls in tetragonal PbTiO_3 . The Hubbard parameter for Ti $3d$ states is determined using the finite-size-corrected polaronic energy-level alignment procedure, yielding stable electron-polaron formation in bulk PbTiO_3 with a trapping energy of -0.06 eV. In the domain-wall supercell, the excess electron localizes on Ti and forms a Ti^{3+} center with an occupied d_{xy} orbital in-gap state. Comparison of bulk-like and near-wall Ti sites shows that their trapping energies differ by only about 0.01 eV, indicating that this neutral domain wall does not provide a significant thermodynamic driving force for electron-polaron segregation. While the Ising-like reversal of the out-of-plane polarization is preserved, the localized electron induces a finite transverse polarization component normal to the wall, enhancing a local Néel-like distortion that is strongest when the polaron is located at the wall. These results show that neutral 180° domain walls in PbTiO_3 do not substantially alter the stability of Ti-centered electron polarons, but they can couple to the polaron-induced lattice distortion through a localized transverse polarization response.

I. INTRODUCTION

Ferroelectric perovskite oxides such as BaTiO_3 , $\text{PbZr}_x\text{Ti}_{1-x}\text{O}_3$, and PbTiO_3 are widely studied for non-volatile memories, sensors, actuators, and capacitor technologies because their spontaneous polarization can be switched by external fields [1–3]. Below the Curie temperature, the paraelectric phase transforms into a polar state with several symmetry-equivalent polarization variants. The crystal therefore subdivides into domains separated by atomically thin domain walls (DWs), which reduce depolarizing fields and elastic energy [4]. Because DWs can be created, displaced, and reconfigured by electric fields, they are increasingly viewed not only as passive microstructural features but also as functional nanoscale elements for domain-wall electronics [5, 6].

The functional response of ferroelectric DWs is strongly affected by defects and charge-compensation mechanisms. Dopants, vacancies, and excess carriers can modify DW mobility, pinning, local conductivity, and polarization structure; consequently, predictive control of ferroelectric properties requires a microscopic understanding of how charged species interact with different DW types [7–12]. This issue is particularly important because ferroelectric DWs may be either neutral, as in side-by-side or head-to-tail configurations, or charged, as in head-to-head and tail-to-tail configurations. Charged DWs carry bound polarization charge and therefore generate local electrostatic potentials that must be compensated [13–16]. One possible compensation mechanism is the accumulation of free carriers at the wall [17, 18]. However, the generally low conductivity and high resistivity of many ferroelectric oxides indicate that compen-

sation can also occur through localized valence changes of lattice ions or through self-trapped carriers [19–21].

Self-trapped carriers, or small polarons, form when an excess electron or hole localizes on an atomic site together with a local lattice distortion [22]. In oxide ferroelectrics, such localization is directly connected to reduction or oxidation of host ions and can therefore set charge-compensation limits and pin the Fermi level [23]. Polarons are thus relevant not only for electronic and optical properties, but also for the response of domain walls to charged defects and non-stoichiometry [24–31]. Recent theoretical and experimental studies have shown that DWs can act as trapping sites for localized charges or charged defects, thereby influencing DW conductivity, pinning, and transport in ferroelectric and ferroelastic materials [10, 21, 32–38]. These results motivate a direct comparison of polaron stability in bulk-like and DW environments.

PbTiO_3 provides a well-defined model system for this purpose. At room temperature, PbTiO_3 adopts the tetragonal $P4mm$ phase after a paraelectric-to-ferroelectric transition at approximately 763 K [39–44]. Its electronic structure and lattice parameters have been extensively characterized, with a band gap of about 3.2–3.6 eV and an experimental tetragonality of $c/a \approx 1.06$ [45–51]. The structure and energetics of neutral 180° DWs in PbTiO_3 have also been investigated previously, showing that PbO-centered walls are energetically favored over TiO_2 -centered walls [52–54]. These properties make PbTiO_3 an appropriate reference material for isolating the interaction between a neutral ferroelectric DW and a localized excess electron.

In bulk tetragonal PbTiO_3 , Ti-centered electron polarons have been studied in detail and are known to correspond to the reduction of Ti^{4+} to Ti^{3+} , with the excess electron localized in Ti $3d$ states [56–58]. In contrast, O-centered hole polarons are energetically unfavorable as shown by DFT calculations [59]. Despite this established

* amirabbasi@mm.tu-darmstadt.de

† albe@mm.tu-darmstadt.de

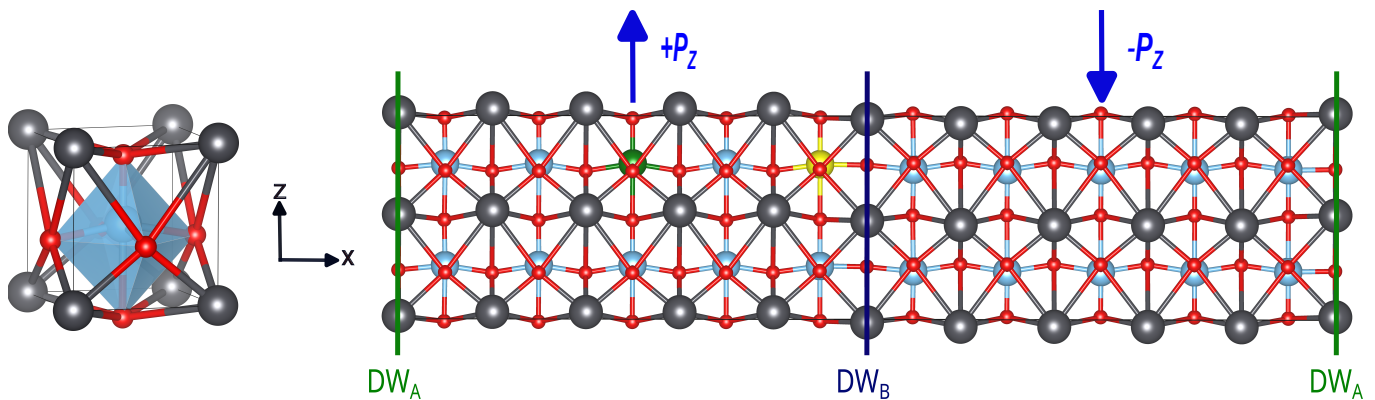


FIG. 1: (Color online) (left panel) Crystal structure of PbTiO_3 primitive cell for up polarization, plotted using VESTA [55]. Ti ions are represented by cyan spheres, Pb ions by black spheres, and O ions by red spheres. Each Ti is surrounded by six oxygen atoms in this system to form a distorted octahedron. The down polarization state is achieved by the rotation of the up polarization state by 180 degrees around the x -axis. (right panel) The optimized $10 \times 2 \times 2$ supercell size of 180° DW. The Green and dark-blue solid lines denote two symmetric DW. Notably, within the DW, the Ti-O bond lengths along the epical direction undergo variations. Similarly, positions of the Pb ions also exhibit changes across the DW. The green and yellow spheres denote the location of the installing electron polaron in bulk and wall regions relative to DW, respectively.

bulk behavior, it remains unclear whether a neutral 180° DW substantially changes the trapping energy of a Ti-centered electron polaron, and whether such a localized carrier modifies the local polarization structure of the wall. This distinction is important: if the DW lowers the polaron trapping energy, it may act as a segregation site for self-trapped electrons; if not, then the polaron remains essentially bulk-like and the neutral wall does not provide a thermodynamic driving force for charge localization.

In this work, we address this question using density functional theory with a Hubbard correction (DFT+ U). We first determine an appropriate U parameter for Ti $3d$ states using a finite-size-corrected level-alignment procedure, since the predicted stability of localized polarons is sensitive to self-interaction errors and finite-size effects [60–62]. We then construct a PbO-centered neutral 180° DW in tetragonal PbTiO_3 and compare Ti-centered electron polarons located in bulk-like and near-wall regions. By analyzing trapping energies, electronic density of states, and local polarization profiles, we determine whether the neutral DW promotes electron-polaron segregation and how the localized charge couples to the Ising-like polarization reversal at the wall.

II. COMPUTATIONAL DETAILS

First-principles calculations were performed using the Vienna *ab initio* simulation package (VASP) [63, 64]. The electron-ion interaction was described by the projector augmented-wave (PAW) method [64, 65], and exchange-correlation effects were treated within the PBEsol form of the generalized-gradient approximation [66, 67]. The valence configurations were $6s^2 6p^2$ for Pb, $3s^2 3p^6 3d^2 4s^2$

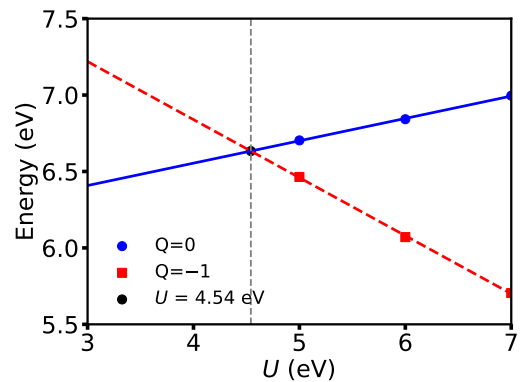


FIG. 2: Hubbard correction $U_{\text{Ti-}3d}$ for a $3 \times 3 \times 3$ supercell with a polaronic state.

for Ti, and $2s^2 2p^4$ for O. Plane-wave cutoff energies of 900 eV and 520 eV were used for primitive-cell and supercell calculations, respectively.

The tetragonal PbTiO_3 primitive cell was initialized from the experimental structure [48]. Both lattice vectors and internal coordinates were relaxed at the PBEsol level. Since the structural tetragonality of PbTiO_3 is sensitive to the choice of exchange-correlation functional, and since adding a Hubbard correction during the structural optimization reduces the PBEsol *tetragonality*, the PBEsol-optimized volume was used as the reference geometry for subsequent calculations. The Hubbard correction was applied in calculations involving excess-charge localization, where self-interaction errors directly affect the stability of the polaronic state. Brillouin-zone sampling was performed using Γ -centered meshes of $10 \times 10 \times 10$ for the primitive cell and $3 \times 3 \times 3$ for

the $3 \times 3 \times 3$ bulk supercell. All ionic relaxations were continued until the residual forces were below 5×10^{-3} eV/Å.

A neutral 180° domain wall was constructed by joining oppositely polarized tetragonal PbTiO_3 domains along the [100] direction, with the spontaneous polarization oriented along [001] (see Fig. 1). The downward-polarized domain was generated by rotating the upward-polarized structure by 180° about the [001] axis. We considered a PbO-centered wall, which is the lower-energy configuration for neutral 180° domain walls in tetragonal PbTiO_3 [52–54]. The pristine wall structure was first relaxed in a $10 \times 1 \times 1$ supercell and then expanded to a $10 \times 2 \times 2$ supercell for the polaron calculations. The corresponding Γ -centered k -point meshes were $2 \times 8 \times 8$ and $2 \times 4 \times 4$, respectively.

Localized electron polarons were generated by adding one excess electron to the supercell and initially constraining the occupation matrix of a selected Ti center. This procedure breaks the symmetry of the delocalized conduction-band state and promotes localization of the excess electron on a chosen Ti site. During the following ionic relaxation, the surrounding Ti–O bonds respond to the localized charge and form the accompanying lattice distortion. After this distortion was established, the occupation constraint was removed and the system was fully re-relaxed self-consistently within DFT+ U . Occupation-matrix control was used to avoid convergence to metastable or delocalized solutions associated with the multi-minimum character of DFT+ U calculations [68].

The Hubbard parameter applied to Ti $3d$ states was not treated as an empirical fitting parameter. Instead, it was determined using the finite-size-corrected level-alignment procedure of Falletta *et al.* [61], in which the polaronic Kohn–Sham level is aligned between the fully occupied and empty charge states after removing spurious electrostatic finite-size contributions (see Fig. 2)). This point is important because the value of U controls the balance between electron localization and delocalization: too small a U leaves excessive self-interaction error and favors an extended conduction-band state, whereas too large a U can over-localize the excess electron.

For the occupied polaron level, the electrostatic correction to the Kohn–Sham eigenvalue is written as

$$\epsilon_{\text{corr}}^{\text{occ}} = -\frac{2}{q} E_{\text{m}}(q, \epsilon_0), \quad (1)$$

whereas for the empty polaron level it is

$$\epsilon_{\text{corr}}^{\text{unocc}} = -\frac{2}{q + q'_{\text{pol}}} E_{\text{m}}(q + q'_{\text{pol}}, \epsilon_\infty). \quad (2)$$

Here, q is the net charge of the simulation cell, $q'_{\text{pol}} = -q(1 - \epsilon_\infty/\epsilon_0)$ is the polarization charge associated with the ionic relaxation around the polaron, and E_{m} is the image-charge correction evaluated using the Freysoldt

scheme [69, 70]. The static dielectric constant ϵ_0 screens the long-range electrostatic interaction of the occupied, relaxed polaron, whereas the high-frequency dielectric constant ϵ_∞ is appropriate for the unoccupied level, for which only the electronic polarization responds. We used the experimental dielectric constants $\epsilon_{\infty,a} = 6.64$, $\epsilon_{\infty,c} = 6.63$, $\epsilon_{0,a} = 106.9$, and $\epsilon_{0,c} = 28.6$ [71]. This procedure yields $U_{\text{Ti-}3d} = 4.54$ eV for Ti $3d$ states.

III. RESULTS AND DISCUSSION

A. Geometry optimization

We start from the geometry optimization of the primitive cell in the tetragonal phase. We use an experimental CIF file [48] as the starting point and optimize both the cell volume and ionic positions. For the study of the tetragonal phase of FE materials like PbTiO_3 , selecting an appropriate pseudopotential approach to approximate the electron-ion interaction and exchange-correlation functional is crucial to achieving a c/a ratio close to the experimental value. PBE functional overestimates the c/a ratio ($c/a=1.23$ [57]), and the addition of U does not significantly improve this discrepancy ($c/a=1.005$ [57]), although the other lattice constants are closer to the experimental measurements ($a = b = 3.98$ Å [57]). In contrast, we find that the PBEsol functional yields a c/a ratio of 1.08, which decreases to 1.01 with the inclusion of U . Given that the PBEsol functional provides a c/a ratio closer to the experimental value, we adopt the PBEsol-derived volume for subsequent calculations. In addition, the U is considered only for optimizing ionic positions in the following analysis when we consider excess charge for formation of polaron. The optimized lattice constants using PBEsol exchange-correlation functional are determined to be $a = b = 3.87$ Å and $c = 4.19$, resulting in a c/a ratio of 1.08. These values show good agreement with the experimental data [48–50] (see Tab. I).

TABLE I: Comparison of experimentally measured and theoretically calculated lattice constants and c/a ratios for the tetragonal phase of PbTiO_3 , highlighting data from various studies in the scientific literature.

Methods	$a = b$ (Å)	c (Å)	c/a
Exp. [49, 51]	3.90	4.15	1.06
Exp. [48]	3.90	4.13	1.06
PBE [57]	3.84	4.72	1.23
PBE+ U [57]	3.98	4.00	1.005
PBEsol+ U	3.94	3.99	1.01
PBEsol	3.87	4.19	1.08

B. Electron-polaron trapping in bulk phase

Prior to investigating the interaction between the electron polaron and the DW, we evaluated the trapping of the polaron on a bulk Ti site using supercells of various sizes. The trapping energy of the electron polaron was evaluated using band-edge reference formulation [59, 72],

$$E_{\text{trap}} = E_{\text{pol}}^{-1} - E_{\text{pristine}}^0 - \epsilon_{\text{CBM}} + E_{\text{corr}}, \quad (3)$$

where E_{pristine}^0 is the energy of the neutral pristine supercell and ϵ_{CBM} is the conduction-band minimum of the corresponding pristine system: In this formulation, the trapping energy converges systematically with supercell size, as shown in Fig. 3. The resulting finite-size-corrected trapping energy converges to -0.06 eV, differing from earlier reported values of -0.16 and -0.13 eV [57, 58]. This discrepancy likely arises from differences in the U parameter applied to Ti-3d orbitals, the exchange-correlation functional, and dielectric constants, as well as the use of the delocalized electron configuration as the reference state in those studies.

Figure 4 displays the density of states (DOS) for the localized (polaronic) charge configurations. It reveals a distinct spin-up state below the Fermi energy, indicative of a stable localized polaron. Our calculations show that the additional electron predominantly occupies the d_{xy} orbital of the Ti ions, contributing a magnetic moment of $1 \mu_B$. Prior to polaron formation, the Ti ion is in the Ti^{4+} oxidation state, with an empty 3d shell. Upon localization, the ion is reduced to Ti^{3+} , adopting a $3d^1$ electronic configuration. The polaron level lies 0.75 eV below the CBM.

C. Electron-polaron on Ti-center: 180° Pb-center DW

We next examine the interaction between a Ti-centered electron polaron and a neutral 180° DW in tetragonal

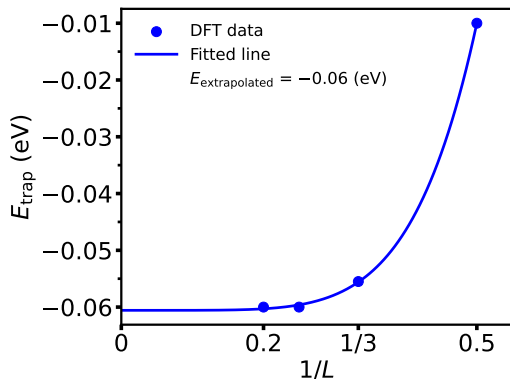


FIG. 3: Polaron trapping energy as a function of inverse supercell size, $(1/L)$, for $L = 2-5$.

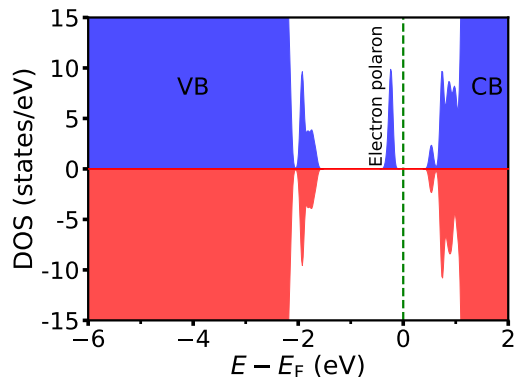


FIG. 4: DOS of the polaron configuration using the corrected $U_{\text{Ti-3d}}$. Blue and red curves denote the spin-up and spin-down channels, respectively. The Fermi energy is set to zero, and the electron-polaron level lies 0.75 eV below the CBM.

PbTiO_3 . The calculations are performed using a $10 \times 2 \times 2$ supercell containing 200 atoms using DFT+ U . The supercell comprises domains with opposite out-of-plane polarization, separated by a Pb-centered 180° DW, as shown in Fig. 1. To distinguish bulk-like and DW-related polaron behavior, the excess electron is localized on Ti sites either far from or close to the DW, indicated by the green and yellow spheres in Fig. 1, respectively. The domain wall formation energy is calculated as

$$\gamma_{\text{DW}} = \frac{E_{\text{DW}} - E_{\text{Bulk}}}{2A}, \quad (4)$$

where E_{DW} and E_{Bulk} are total energies of the supercell structure containing DW and bulk, respectively. A is the area of the domain wall. The resulting value of $\gamma_{\text{DW}} = 144 \text{ mJ m}^{-2}$, is consistent with the result of previous first-principles calculations (128 and 132 mJ m^{-2}) for 180° domain walls in the Pb-O plane of tetragonal PbTiO_3 [52, 53].

To characterize the local polarization profile across the DW, we evaluate the polarization associated with each Ti-centered unit using

$$P_i = \frac{e}{\Omega} \sum_j \frac{q_j}{n_j} (r_i^j - r_i^{\text{Ti}}), \quad (5)$$

where Ω is the unit-cell volume, n_j is the multiplicity of atomic species j , and $r_i^j - r_i^{\text{Ti}}$ denotes the displacement of atom j relative to the central Ti ion along Cartesian direction i . The Born effective charges are taken from Ref. 73, with $q_{\text{Ti}} = +6.71$, $q_{\text{Pb}} = +3.92$, $q_{\text{O}_{\text{apical}}} = -5.51$, and $q_{\text{O}_{\text{equatorial}}} = -2.56$.

The resulting polarization profiles are shown in Fig. 5. In the pristine DW structure, the polarization is dominated by the out-of-plane Ising component, P_z , which changes sign abruptly across the wall. The corresponding DW width is confined to approximately one prim-

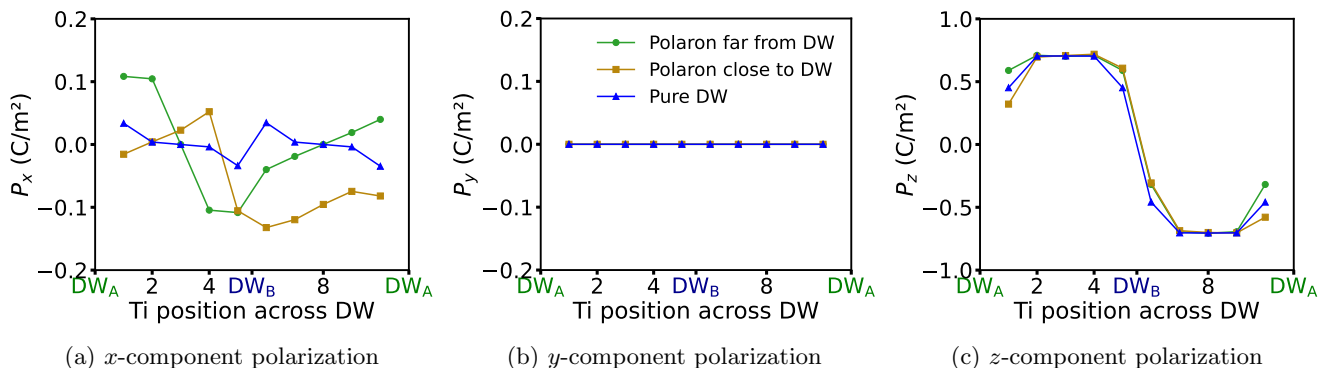


FIG. 5: (Color online) Polarization components across a neutral 180° Pb-centered domain wall in PbTiO_3 . Panels show (a) P_x , (b) P_y , and (c) P_z versus Ti position across the supercell. In the pure structure, P_y remains negligible, while a small wall-normal Néel component, P_x , appears near the domain wall; P_z dominates and reverses sign across the 180° wall. Adding a localized electron polaron preserves the P_z and P_y profiles, whereas a finite wall-normal component, P_x , develops at the polaron site.

itive unit cell ($\sim 3.87 \text{ \AA}$), consistent with previous first-principles calculations for Pb-centered 180° DWs in PbTiO_3 [52]. The transverse in-plane component, P_y , remains negligible throughout the supercell. By contrast, a small wall-normal Néel-like component, P_x , develops in the vicinity of the DW, in agreement with the behavior reported by Behera *et al.* [53]. Its maximum value in our calculation, $P_x = 0.035 \text{ C m}^{-2}$, is close to the previously reported value of 0.024 C m^{-2} . The calculated saturation value of the Ising component, $P_z \approx 0.7 \text{ C m}^{-2}$, also agrees well with experimental values ($0.5\text{--}1.0 \text{ C m}^{-2}$) [74, 75] and with zero-temperature first-principles predictions ($0.87\text{--}1.14 \text{ C m}^{-2}$) [52, 76–79].

Introducing a localized electron polaron on a Ti site leaves the overall Ising polarization profile essentially unchanged. In particular, the reversal of P_z across the DW and the negligible transverse component P_y are retained for polarons both far from and close to the DW. The main structural response is instead a localized enhancement of the wall-normal polarization component at the polaron site. For a polaron located far from the DW, P_x reaches 0.11 C m^{-2} , whereas for a polaron located close to the DW the maximum value is reduced to 0.05 C m^{-2} . Thus, the Ti-centered electron polaron induces a local wall-normal polar distortion without significantly modifying the underlying 180° Ising DW profile. This behavior is analogous to the local transverse or wall-normal polar distortions previously reported for point defects such as oxygen vacancies interacting with ferroelectric DWs [80, 81].

Finally, we evaluate the energetic stability of the Ti-centered electron polaron at two representative positions, one in a bulk-like region and one close to the DW. The occupied polaronic state is located 0.64 eV below the conduction-band minimum (CBM) for the bulk-like Ti site and 0.59 eV below the CBM for the Ti site near the DW. The corresponding trapping energies are -0.04 eV and -0.03 eV , respectively, indicating that electron-

polaron formation is favorable in both cases.

The trapping energies, however, differ by only 0.01 eV . This very small energy difference is within the expected uncertainty associated with finite-size and self-interaction effects in the elongated $10 \times 2 \times 2$ DW supercell. In particular, the bulk-like trapping energy obtained in this geometry differs from the value calculated for the more isotropic $3 \times 3 \times 3$ bulk supercell, reflecting residual self-interaction of the localized excess electron in the DW supercell. We therefore do not interpret the small difference between the bulk-like and near-DW trapping energies as a meaningful site preference. Rather, these results show that the neutral Pb-centered 180° DW provides no significant thermodynamic driving force for Ti-centered electron-polaron segregation.

IV. CONCLUSION

In this work, we investigated the interaction of electron polarons with a 180° domain wall in PbTiO_3 . While hole polarons on oxygen sites are not expected for PbTiO_3 [57], electron localizes on Ti centers with a trapping energy of -0.06 eV . In the domain-wall supercell, the Ti-centered electron polaron produces a local enhancement of the wall-normal polarization component, while the main out-of-plane Ising polarization profile remains essentially unchanged. The occupied polaronic level lies below the conduction-band minimum, but the calculated trapping energies are small. In particular, the trapping energies for a bulk-like Ti site and a Ti site close to the domain wall differ by only 0.01 eV .

This behavior contrasts with what has been reported for oxygen vacancies at a 180° domain wall in PbTiO_3 . Oxygen vacancies are point defects that can couple more directly to the local wall structure and have been shown to induce transverse or wall-normal polarization components at domain walls [82]. In this respect, the Ti-

centered electron polaron produces a qualitatively similar local polarization response: it also generates a finite wall-normal component, P_x , at the polaron site. However, the energetic effect is much weaker for the isolated electron polaron (10 meV vs 250 meV). While oxygen vacancies can act as stronger structural perturbations and may promote defect accumulation or local wall modification, the electron polaron studied here mainly induces a local polar distortion without appreciable segregation to the neutral wall.

ACKNOWLEDGEMENT

Authors acknowledge financial support from the Collaborative Research Center FLAIR (Fermi level engineering applied to oxide electroceramics), funded by the German Research Foundation (DFG) under Project-ID No. 463184206-SFB 1548 (project A02). Lichtenberg and Paderborn Supercomputing Centers are gratefully acknowledged by MA as the providers of needed computing facilities. The guidelines provided by Prof. Julia Wiktor, Dr. Lorenzo Villa, Dr. Marcel Sadowski, Dr. Gustav Bhilmayer, Dr. Zhenbang Dai, Prof. Feliciano Giustino and Dr. Stefano Falletta are highly valued by MA.

-
- [1] J. F. Scott, *Science* **315**, 954 (2007).
- [2] M. Acosta, N. Novak, V. Rojas, S. Patel, R. Vaish, J. Koruza, J. Rossetti, G. A., and J. Rödel, *Appl. Phys. Rev.* **4**, 041305 (2017).
- [3] P. Muralt, *IEEE Trans. Ultrason. Ferroelectr. Freq. Control.* **47**, 903 (2002).
- [4] A. K. Tagantsev, L. E. Cross, and J. Fousek, *Domains in Ferroic Crystals and Thin Films* (Springer New York).
- [5] E. K. Salje, *Phase Trans.* **86**, 2 (2013).
- [6] D. Meier and S. M. Selbach, *Nat. Rev. Mat.* **7**, 157 (2022).
- [7] D. Lee, H. Xu, V. Dierolf, V. Gopalan, and S. R. Phillpot, *Appl. Phys. Lett.* **98**, 092903 (2011).
- [8] G. F. Nataf, M. Guennou, J. M. Gregg, D. Meier, J. Hlinka, E. K. H. Salje, and J. Kreisel, *Nat. Rev. Mat.* **2**, 634 (2020).
- [9] A. Chandrasekaran, D. Damjanovic, N. Setter, and N. Marzari, *Phys Rev B* **88**, 214116 (2013).
- [10] A. Bencan, G. Drazic, H. Ursic, M. Makarovic, M. Komelj, and T. Rojac, *Nat. Commun.* **11**, 1762 (2020).
- [11] A. J. Klomp, R. Khachatryan, T. Wallis, K. Albe, and A. Grünebohm, *Phys. Rev. Mater.* **6**, 104411 (2022).
- [12] P. Marton, M. Paściak, M. A. P. Gonçalves, O. Novák, J. Hlinka, R. Beanland, and M. Alexe, *Comm. Mat.* **6**, 161 (2025).
- [13] G. Catalan, J. Seidel, R. Ramesh, and J. F. Scott, *Rev. Mod. Phys.* **84**, 119 (2012).
- [14] D. Meier, *J. Phys.: Condens. Matter* **27**, 463003 (2015).
- [15] P. Maksymovych, J. Seidel, Y. H. Chu, P. Wu, A. P. Bad-dorf, L.-Q. Chen, S. V. Kalinin, and R. Ramesh, *Nano Lett.* **11**, 1906 (2011).
- [16] G. Tian, W. Yang, X. Song, D. Zheng, L. Zhang, C. Chen, P. Li, H. Fan, J. Yao, D. Chen, Z. Fan, Z. Hou, Z. Zhang, S. Wu, M. Zeng, X. Gao, and J.-M. Liu, *Adv. Funct. Mater.* **29**, 1807276 (2019).
- [17] Y. Zuo, Y. A. Genenko, and B.-X. Xu, *J. Appl. Phys.* **116**, 044109 (2014).
- [18] T. Sluka, A. K. Tagantsev, D. Damjanovic, M. Gureev, and N. Setter, *Nat. Commun.* **3**, 748 (2012).
- [19] J. Seidel, L. W. Martin, Q. He, Q. Zhan, Y.-H. Chu, A. Rother, M. E. Hawkrige, P. Maksymovych, P. Yu, M. Gajek, N. Balke, S. V. Kalinin, S. Gemming, F. Wang, G. Catalan, J. F. Scott, N. A. Spaldin, J. Orenstein, and R. Ramesh, *Nat. Mater.* **8**, 229 (2009).
- [20] N. S. Bein, P. Machado, M. Coll, F. Chen, M. Makarovic, T. Rojac, and A. Klein, *J. Chem. Phys. Lett.* **10**, 7071 (2019).
- [21] T. Rojac, A. Bencan, G. Drazic, N. Sakamoto, H. Ursic, B. Jancar, G. Tavcar, M. Makarovic, J. Walker, B. Malic, and D. Damjanovic, *Nat. Mater.* **16**, 322 (2017).
- [22] C. Franchini, M. Reticcioli, M. Setvin, and U. Diebold, *Nat. Rev. Mat.* **6**, 560 (2021).
- [23] A. Klein, K. Albe, N. Bein, O. Clemens, K. A. Creutz, P. Erhart, M. Frericks, E. Ghorbani, J. P. Hofmann, B. Huang, B. Kaiser, U. Kolb, J. Koruza, C. Kübel, K. N. S. Lohaus, J. Rödel, J. Rohrer, W. Rheinheimer, R. A. D. Souza, V. Streibel, A. Weidenkaff, M. Widemeyer, B.-X. Xu, and H. Zhang, *J. Electroceram.* **51**, 147 (2023).
- [24] J. B. Varley, A. Janotti, C. Franchini, and C. G. Van de Walle, *Phys Rev B* **85**, 081109 (2012).
- [25] B. Faust, H. Müller, and O. Schirmer, *Ferroelectrics* **153**, 297 (1994).
- [26] F. Ambrosio, J. Wiktor, F. De Angelis, and A. Pasquarello, *Energy & Env. Sci.* **11**, 101 (2018).
- [27] M. Friedrich, W. G. Schmidt, A. Schindlmayr, and S. Sanna, *Phys. Rev. Mater.* **1**, 054406 (2017).
- [28] O. F. Schirmer, *J. Phys.: Condens. Matter* **18**, R667 (2006).
- [29] O. F. Schirmer, M. Imlau, C. Merschjann, and B. Schoke, *J. Phys.: Condens. Matter* **21**, 123201 (2009).
- [30] V. S. Vikhnin, R. I. Eglitis, S. E. Kapphan, G. Borstel, and E. A. Kotomin, *Phys Rev B* **65**, 104304 (2002).
- [31] F. Ambrosio and J. Wiktor, *J. Chem. Phys. Lett.* **10**, 7113 (2019).
- [32] Y. Xu, P. Sharma, H. Wen, D. Zhang, C. Kong, Z. Yan, S. L. Chang, and J. Seidel, *Adv. Funct. Mater.* **34**, 2400420 (2024).
- [33] S. Körbel, J. Hlinka, and S. Sanvito, *Phys Rev B* **98**, 100104 (2018).
- [34] S. Y. Xiao, T. Kämpfe, Y. M. Jin, A. Haußmann, X. M. Lu, and L. M. Eng, *Phys. Rev. Appl.* **10**, 034002 (2018).
- [35] M. Schröder, A. Haußmann, A. Thiessen, E. Soergel, T. Woike, and L. M. Eng, *Adv. Funct. Mater.* **22**, 3936 (2012).
- [36] D. Meier, J. Seidel, A. Cano, K. Delaney, Y. Kumagai, M. Mostovoy, N. A. Spaldin, R. Ramesh, and M. Fiebig, *Nat. Mater.* **11**, 284 (2012).

- [37] E. A. Eliseev, A. N. Morozovska, G. S. Svechnikov, P. Maksymovych, and S. V. Kalinin, *Phys Rev B* **85**, 045312 (2012).
- [38] F. Kluibenschedl, G. M. Koutentakis, R. Alhyder, and M. Lemeshko, *Phys Rev Lett* **134**, 096302 (2025).
- [39] N. Siron, B. Ravel, Y. Yacoby, E. A. Stern, F. Dogan, and J. J. Rehr, *Phys Rev B* **50**, 13168 (1994).
- [40] A. M. Glazer and S. A. Mabud, *Acta Cryst. B* **34**, 1065 (1978).
- [41] A. García and D. Vanderbilt, *Phys Rev B* **54**, 3817 (1996).
- [42] R. J. Nelmes, R. O. Piltz, W. F. Kuhs, Z. Tun, and R. R. and, *Ferroelectrics* **108**, 165 (1990).
- [43] M. D. Fontana, H. Idrissi, and K. Wojcik, *Europhys. Lett.* **11**, 419 (1990).
- [44] G. Burns and B. A. Scott, *Phys Rev B* **7**, 3088 (1973).
- [45] D. I. Bilc, R. Orlando, R. Shaltaf, G.-M. Rignanese, J. Íñiguez, and P. Ghosez, *Phys Rev B* **77**, 165107 (2008).
- [46] R. Schafrank, S. Li, F. Chen, W. Wu, and A. Klein, *Phys Rev B* **84**, 045317 (2011).
- [47] K. van Benthem, C. Elsässer, and R. H. French, *J. Appl. Phys.* **90**, 6156 (2001).
- [48] J. Joseph, T. M. Vimala, V. Sivasubramanian, and V. R. K. Murthy, *J. Mater. Sci.* **35**, 1571 (2000).
- [49] W. Dmowski, T. Egami, L. Farber, and P. K. Davies, *AIP Conf. Prof.* **582**, 33 (2001).
- [50] J. A. Rodriguez, A. Etxebarria, L. González, and A. Maiti, *J. Chem. Phys.* **117**, 2699 (2002).
- [51] T. Yamanaka, Y. Nakamoto, M. Ahart, and H.-k. Mao, *Phys Rev B* **97**, 144109 (2018).
- [52] B. Meyer and D. Vanderbilt, *Phys Rev B* **65**, 104111 (2002).
- [53] R. K. Behera, C. W. Lee, D. Lee, A. N. Morozovska, S. B. Sinnott, A. Asthagiri, V. Gopalan, and S. R. Phillpot, *J. Phys.: Condens. Matter* **23**, 175902 (2011).
- [54] S. Pöykkö and D. Chadi, *Appl. Phys. Lett.* **75**, 2830 (1999).
- [55] K. Momma and F. Izumi, *J. Appl. Crystallogr.* **44**, 1272 (2011).
- [56] R. I. Eglitis, E. A. Kotomin, V. A. Trepakov, S. E. Kaphan, and G. Borstel, *J. Phys.: Condens. Matter* **14**, L647 (2002).
- [57] E. Ghorbani, L. Villa, P. Erhart, A. Klein, and K. Albe, *Phys. Rev. Mater.* **6**, 074410 (2022).
- [58] D. Windsor and H. Xu, *Phys. Rev. Mater.* **8**, 094406 (2024).
- [59] P. Erhart, A. Klein, D. Åberg, and B. Sadigh, *Phys Rev B* **90**, 035204 (2014).
- [60] M. Cococcioni and S. de Gironcoli, *Phys Rev B* **71**, 035105 (2005).
- [61] S. Falletta, J. Wiktor, and A. Pasquarello, *Phys Rev B* **102**, 041115 (2020).
- [62] S. Falletta and A. Pasquarello, *npj Computational Materials* **8**, 263 (2022).
- [63] G. Kresse and J. Furthmüller, *Comp. Mat. Sci.* **6**, 15 (1996).
- [64] G. Kresse and D. Joubert, *Phys Rev B* **59**, 1758 (1999).
- [65] P. E. Blöchl, *Phys Rev B* **50**, 17953 (1994).
- [66] J. P. Perdew, K. Burke, and M. Ernzerhof, *Phys Rev Lett* **77**, 3865 (1996).
- [67] J. P. Perdew, A. Ruzsinszky, G. I. Csonka, O. A. Vydrov, G. E. Scuseria, L. A. Constantin, X. Zhou, and K. Burke, *Phys Rev Lett* **100**, 136406 (2008).
- [68] J. P. Allen and G. W. Watson, *Phys. Chem. Chem. Phys.* **16**, 21016 (2014).
- [69] C. Freysoldt, J. Neugebauer, and C. G. Van de Walle, *Phys Rev Lett* **102**, 016402 (2009).
- [70] C. Freysoldt, B. Grabowski, T. Hickel, J. Neugebauer, G. Kresse, A. Janotti, and C. G. Van de Walle, *Rev. Mod. Phys.* **86**, 253 (2014).
- [71] C. M. Foster, Z. Li, M. Grimsditch, S.-K. Chan, and D. J. Lam, *Phys Rev B* **48**, 10160 (1993).
- [72] N. Österbacka, P. Erhart, S. Falletta, A. Pasquarello, and J. Wiktor, *Chem. Mater.* **32**, 8393 (2020).
- [73] W. Zhong, R. D. King-Smith, and D. Vanderbilt, *Phys Rev Lett* **72**, 3618 (1994).
- [74] M. E. Lines and A. M. Glass, *Principles and Applications of Ferroelectrics and Related Materials* (Oxford University Press, 2001).
- [75] T. Abe, S. Kim, C. Moriyoshi, Y. Kitanaka, Y. Noguchi, H. Tanaka, and Y. Kuroiwa, *Appl. Phys. Lett.* **117**, 252905 (2020).
- [76] E. Tadmor, U. Waghmare, G. Smith, and E. Kaxiras, *Acta Mater.* **50**, 2989 (2002).
- [77] G. Sághi-Szabó, R. E. Cohen, and H. Krakauer, *Phys Rev Lett* **80**, 4321 (1998).
- [78] M. Kingsland, K. A. Lynch, S. Lisenkov, X. He, and I. Ponomareva, *Phys. Rev. Mater.* **4**, 073802 (2020).
- [79] Y. Zhang, J. Sun, J. P. Perdew, and X. Wu, *Phys Rev B* **96**, 035143 (2017).
- [80] U. Petralanda, M. Kruse, H. Simons, and T. Olsen, *Phys Rev Lett* **127**, 117601 (2021).
- [81] S. Tomoda, T. Shimada, T. Ueda, J. Wang, and T. Kitamura, *Mech. Eng. J.* **2**, 15 (2015).
- [82] L. He and D. Vanderbilt, *Phys Rev B* **68**, 134103 (2003).